ADVANCED FUNCTIONAL MATERIALS
www.afm-journal.de

Designing Geometric Degrees of Freedom in ReO_3-Type Coordination Polymers

*Stefan Burger, Karina Hemmer, David C. Mayer, Pia Vervoorts, Dominik Daisenberger, Jan K. Zaręba, and Gregor Kieslich**

Engineering the interplay of structural degrees of freedom that couple to external stimuli such as temperature and pressure is a powerful approach for material design. New structural degrees of freedom expand the potential of the concept, and coordination polymers as a chemically versatile material platform offer fascinating possibilities to address this challenge. Here, we report a new class of perovskite-like AB_2X_6 coordination polymers based on a $[BX_3]^-$ ReO_3-type host network ($[Mn(C_2N_3)_3]^-$), in which the spatial orientation of divalent A^{2+} cations ($[R_3N(CH_2)_nNR_3]^{2+}$) with separated charge centers that bridge adjacent ReO_3-cavities is introduced as a new geometric degree of freedom. Herringbone and head-to-tail order pattern of $[R_3N(CH_2)_nNR_3]^{2+}$ cations are obtained by varying the separator length *n* and, together with distortions of the pseudocubic $[BX_3]^-$ network, they determine the materials' stimuli-responsive behavior such as counterintuitive large negative compressibility and uniaxial negative thermal expansion. This new family of coordination polymers highlights the chemists' capabilities of designing matter on a molecular level to address macroscopic material functionality and underpins the opportunities of the design of structural degrees of freedom as a conceptual framework for rational material synthesis in the future.

1. Introduction

Dense and porous coordination polymers are a chemically versatile material platform and harbor a wealth of fascinating properties of academic and technological relevance. Recent examples are their application in next-generation water harvesting[1] and cooling technologies,[2] the observation of counter-intuitive material responses such as negative gas adsorption[3] and colossal negative linear compressibility[4] and negative thermal expansion,[5] enzyme-type molecular recognition[6] and their melting behavior as important intermediate state for the fabrication of functional glasses[7] amongst many more. These examples illustrate the importance of fundamental research related to the materials' stimuli-responsive behavior. It involves the study of material responsiveness for a knowledge-based improvement of existing material functionality, and provides the scientific basis for new material functions and potential next-generation technologies in the future.

In the pursuit to translate between synthetic chemistry and the underlying material's free energy surface which defines material responsiveness,[8,9] the decomposition of a material's structure in terms of available structural and electronic degrees of freedom has proved powerful.[10–12] In coordination polymers, the available structural degrees of freedom, that is, structural distortions that couple to external stimuli such as temperature and pressure, play the most prominent role due to relatively low densities and, when carefully engineered, can introduce new stimuli-responsive properties such as electric polarization that couples to an electric field.[13] The simple use of molecular scaffolds to synthesize 1D, 2D, or 3D coordination polymers introduces new unconventional structural degrees of freedom compared to solid-state inorganics. Examples are orientational degrees of freedom related to order–disorder phase transitions in the barocaloric $[(C_3H_7)_4N]Mn(C_2N_3)_3$ and photovoltaic absorber $[CH_3NH_3]PbI_3$,[2,14] large translational network deformations in the flexible metal-organic frameworks (MOFs) CUK-1 and DMOF-1 derivatives[15,16] with potential in mechanical energy storage processes, and rotational molecular motions in amphidynamic MOFs[17] as a basis for coordination polymer-based molecular machines. The interpretation of a material's

S. Burger, K. Hemmer, D. C. Mayer, P. Vervoorts, G. Kieslich
Department of Chemistry
Technical University of Munich
Lichtenbergstrasse 4, 85748 Garching, Germany
E-mail: gregor.kieslich@tum.de
D. Daisenberger
Diamond Light Source
Harwell Science and Innovation Campus
Didcot, Oxfordshire OX11 ODE, UK
J. K. Zaręba
Institute of Advanced Materials
Wrocław University of Science and Technology
Wybrzeże Wyspiańskiego 27, Wrocław 50-370, Poland
The ORCID identification number(s) for the author(s) of this article can be found under https://doi.org/10.1002/adfm.202205343.

DOI: 10.1002/adfm.202205343

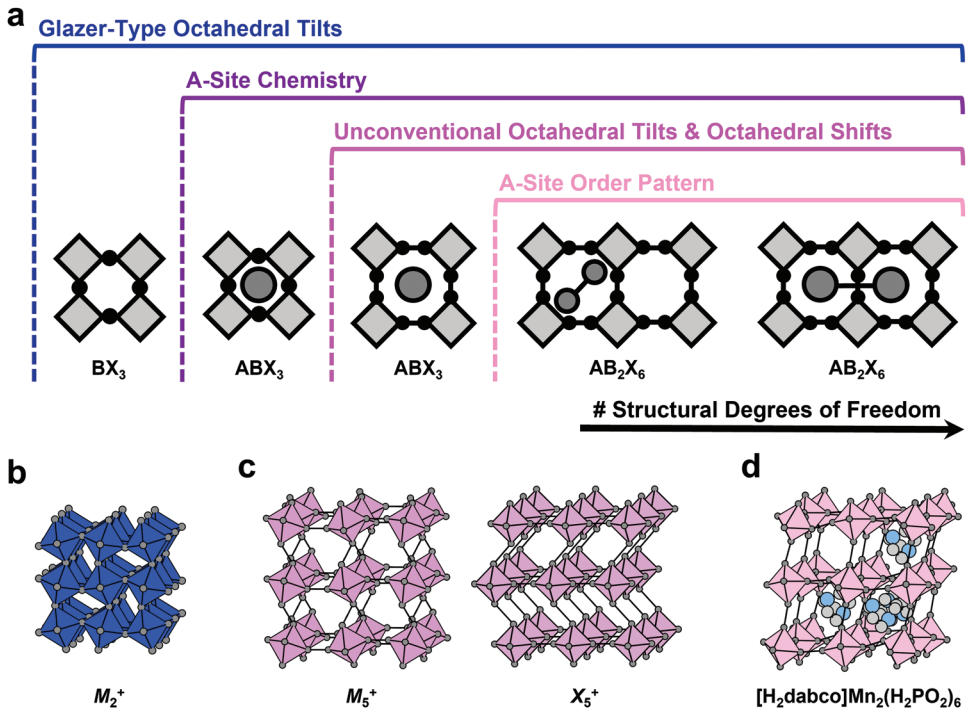

Figure 1. Structural degrees of freedom in ReO_3-type coordination polymers. a) In inorganic ReO_3-type materials and inorganic perovskites Glazer-type octahedral tilts can occur. The use of molecular X-site anions in molecular perovskites makes unconventional octahedral tilts and shifts accessible, and A^{2+} cations such as $[H_2dabco]^{2+}$ in $[H_2dabco]Mn_2(H_2PO_2)_6$ introduce the possibility of various A-site vacancy order pattern. In this work, A^{2+}-site cations with separated charges are used to form AB_2X_6-type materials, adding a new structural degree of freedom related to their spatial orientation within the ReO_3-type network. b) The M_2^+ Glazer-type tilt. c) An unconventional tilt (M_5^+) and shift (X_5^+). d) The crystal structure of $[H_2dabco]Mn_2(H_2PO_2)_6$ is shown with emphasis on the empty voids within the $[Mn(H_2PO_2)_3]^-$ network. Note, for describing the distortion modes of the ReO_3-type network the Bradley–Cracknel notation ($k_\#^+$) is used and that phosphorus and hydrogen atoms are omitted in the structure of $[H_2dabco]Mn_2(H_2PO_2)_6$ for clarity; color code: gray: C, light blue: N.

structure into structural degrees of freedom is capable of conceptualizing current and past research progress related to stimuli-responsive properties of coordination polymers in a concise framework, and in looking forward, engineering the interplay of several structural degrees of freedom shows large opportunities for designing materials with targeted and potentially new stimuli-responsive properties. Therefore, the search for new structural degrees of freedom and their synthetic integration to systematically direct material behavior is an active field of research, either explicitly or implicitly, and the chemical diversity of coordination polymers such as MOFs, Prussian blue analogues and ABX_3 molecular perovskites offer exciting opportunities in this context. The discovery of hidden vacancy networks in Prussian Blue analogues,[18] the introduction of foldable nets[19] and geometry mismatch as concepts,[20] the synthesis of MOFs with frustrated metal-nodes and linker molecules with various internal conformations,[6,21] the categorization of unconventional tilts and shifts in molecular perovskites,[13] and the search for aperiodic MOFs[22] are a few important examples in this context.

ABX_3 molecular perovskites[23] such as $[(NH_2)_2CH]Mn(H_2PO_2)_3$,[24] $[(C_3H_7)_4N]Mn(C_2N_3)_3$,[25] and $[(CH_3)_2NH_2]Zn(HCO_2)_3$[26] are formally a subclass of coordination polymers and exhibit various unconventional structural degrees of freedom. Their structures are based on the well-known perovskite motif where the molecular A-site cation sits in the void of a 3D $[BX_3]^-$ ReO_3-like network. Compared to inorganic perovskites, the use of molecular A- and/or X-site ions introduces unconventional octahedral tilts and shifts,[27] molecular order-disorder phase transitions as a function of temperature[28] and pressure,[29] complex structural phase transition behavior driven by collective changes in atomic vibration,[30] and polymorphism based on conformational isomerism of the B-X connectivity,[31] see **Figure 1**. Initially, unconventional degrees of freedom in molecular perovskites were in the center of fundamental research questions, but recent developments in the field of barocalorics,[32] multiferroics,[33] and improper ferroelectrics[13] highlight the possibilities of manipulating useful macroscopic properties through their targeted variation. When looking for synthetic strategies to integrate new structural degrees of freedom in molecular perovskites, it is important to emphasize that all current structural degrees of freedom originate from the use of molecular building units per sé rather than elaborate synthetic approaches.

Here we apply a crystal structure engineering strategy introducing novel geometric degrees of freedom in a ReO_3-type host network. The synthesis of AB_2X_6 coordination polymers is reported, in which molecular A^{2+} cations with separated positive charges bridge two adjacent cavities of the host network, extending the structural chemistry of ReO_3-type networks with an additional geometric structural motif. The resulting AB_2X_6-materials are conceptually related to ABX_3 molecular

perovskites which guides interpretation of their crystal chemistry. The A^{2+} cations' order pattern depend on their chemical nature and act as property-directing factor, determining the materials' mechanical properties such as thermal expansion behavior and compressibility.

2. Results and Discussion

2.1. Crystal Structure Engineering Methodology

In the pursuit to introduce new geometric degrees of freedom in a ReO_3-type network, the material $[H_2dabco]Mn_2(H_2PO_2)_6$ ($[H_2dabco]^{2+}$ = 1,4-diazabicyclo[2.2.2]octane-1,4-diium) is an important starting point.[24] The use of the divalent cation $[H_2dabco]^{2+}$ leads to a material in which half of the voids within the 3D ReO_3-type $[Mn(H_2PO_2)_3]^-$ cages are occupied, that is, a perovskite-type structure with ordered A-site vacancies, see Figure 1d. Inspired by this example, the use of a divalent A-site cation with separated charge centers, suitable to bridge two pseudocubic $[BX_3]^-$ cages, can be envisaged, which introduces an additional geometric degree of freedom related to the spatial distribution of divalent A-site cations within the 3D $[BX_3]^-$ host network.

The challenge in synthesizing an AB_2X_6 coordination polymer where the divalent A-site cation bridges two $[BX_3]^-$-type cages is the identification of a suitable A-B-X permutation. We use $[C_2N_3]^-$ as X-site anion and Mn^{2+} as B-site divalent metal, a combination that has proved robust for the synthesis of various molecular perovskites with comparably large A-site cations such as $[(C_3H_7)_4N]Mn(C_2N_3)_3$,[25] $[(C_7H_7)(C_4H_9)_3N]Mn(C_2N_3)_3$,[34] and $[(C_3H_7)_3(CH_3)N]Mn(C_2N_3)_3$.[31] On the A-site, a divalent cation must be chosen which exhibits two spatially separated positive charges that can bridge two ReO_3-type $[Mn(C_2N_3)_3]^-$ cages. A divalent A-site cation fulfilling these requirements is the cation $[R_3N(CH_2)_nNR'_3]^{2+}$, where n determines the charge separation distance, and R and R' provide chemical control over the bulkiness of the cation through alkyl chain length, see **Figure 2**a. For the size of R and R', a n-propyl group ($R = -C_3H_7$) seems suitable, resembling the situation in $[(C_3H_7)_4N]Mn(C_2N_3)_3$. Looking at the parameter n, a good separation between the charge centers is expected for $n > 2$. Therefore, $[(C_3H_7)_3N(CH_2)_4N(C_3H_7)_3]^{2+}$ (= $TPC4TP^{2+}$) and $[(C_3H_7)_3N(CH_2)_5N(C_3H_7)_3]^{2+}$ (= $TPC5TP^{2+}$) are promising divalent A-site cations which were synthesized by standard nucleophilic substitution strategies, see Figure S1, Supporting Information. Subsequently, the synthesis of the coordination polymers $[TPC4TP]Mn_2(C_2N_3)_6$ and $[TPC5TP]Mn_2(C_2N_3)_6$ was performed by following an established slow crystallization procedure. For instance, in a typical reaction the precursors $[TPC4TP]Br_2$, $Mn(NO_3)_2 \cdot 4H_2O$ and $Na(C_2N_3)$ are mixed in a water/ethanol mixture. After several days, the formation of single crystals can be observed, see Figure S2, Supporting Information for details.

2.2. Structure and Pattern Analysis

Single crystal X-ray diffraction was used for structure solution, see Tables S2 and S3; Figures S11 and S12, Supporting Information for details of data collection, full crystallographic data and details on structure model discussion. Both compounds crystallize in the monoclinic crystal system and $[TPC4TP]Mn_2(C_2N_3)_6$ in a noncentrosymmetric space-group which was confirmed by second harmonic generation, see Figure S33, Supporting Information for experimental details. A combined TG/DSC analysis shows the absence of a phase transition over the whole stability range, see Figures S7 and S8, Supporting Information. Both materials adopt a 3D ReO_3-type $[Mn(C_2N_3)_3]^-$ coordination network where all Mn^{2+} atoms are octahedrally coordinated by N atoms and linked to their neighbouring Mn^{2+} atoms via six μ-1,5-$[C_2N_3]^-$ bridges. The A-site cations $TPC4TP^{2+}$ and $TPC5TP^{2+}$ are incorporated into the 3D network for charge balance, with one positive charge sitting in each void of a ReO_3-type cage. Therefore, the divalent A-site cations bridge adjacent pseudocubic ReO_3-type cages, see Figure 2b,d. Similar to molecular perovskites, active rigid unit modes in the ReO_3 network are possible and a distortion mode analysis of the 3D $[Mn(C_2N_3)_3]^-$ network reveals the presence of primary order parameters distinctive for dicyanamide-based molecular perovskites,[27] see Supporting Information for full details of the mode analysis.

An intuitive description of both compounds starts from an ABX_3 molecular perovskite where $-(CH_2)_n-$ is used to link two adjacent A-site cations. The introduction of such a $-(CH_2)_n-$ link as a spacer introduces the spatial orientation of the A^{2+} within the $[Mn(C_2N_3)_3]^-$ network as a new structural degree of freedom which is geometric in nature. For $[TPC4TP]Mn_2(C_2N_3)_6$ and $[TPC5TP]Mn_2(C_2N_3)_6$ both A^{2+} cations exhibit 2D order patterns within the 3D ReO_3-type network, that is, they bridge $[Mn(C_2N_3)_3]^-$ cages in two dimensions but not in the third. In $[TPC4TP]Mn_2(C_2N_3)_6$ a herringbone-type order of $TPC4TP^{2+}$ is observed with an AB stacking of individual 2D layers, where B is shifted one pseudocubic unit along one dimension of the 2D layer. For the A-site cation in $[TPC5TP]Mn_2(C_2N_3)_6$ an order pattern is found that we describe as head-to-tail, with head equal to tail, and a AA stacking sequence, see Figure 2c,e; Figures S13 and S15, Supporting Information. Therefore, A^{2+} cations' order pattern and octahedral tilt pattern in $[TPC4TP]Mn_2(C_2N_3)_6$ and $[TPC5TP]Mn_2(C_2N_3)_6$ depend on the chemical identity of the $[R_3N(C_nH_{2n})NR_3]^{2+}$ cation.

The A^{2+} cations' order pattern can be rationalized based on chemical intuition. For $TPC4TP^{2+}$ the length seems to perfectly match the available space within the $[Mn(C_2N_3)_3]^-$ host network. This results in a 2D herringbone pattern where dispersion interactions between R of neighboring cations are presumably maximized. The AB stacking of different layers further suggests that this is achieved by placing one A^{2+} cation in vicinity to a maximum number of other A^{2+} cations. Adding another $-CH_2-$ unit significantly increases the length of the A^{2+} cation, and the dominating factor that determines the order pattern is the reduction of adverse steric interactions between neighboring A^{2+} cations. Due to the size of $TPC5TP^{2+}$ the herringbone pattern seems unfavorable since some of the propyl-chains reach into neighboring $[BX_3]^-$-cages. Instead, $TPC5TP^{2+}$ cations order parallel and lie skewed in the network to minimize unfavorable steric interactions with neighboring A-site cations which is not possible in the herringbone motif, see Figure 2. The distortion of the $[B_2X_6]^-$ cuboid along

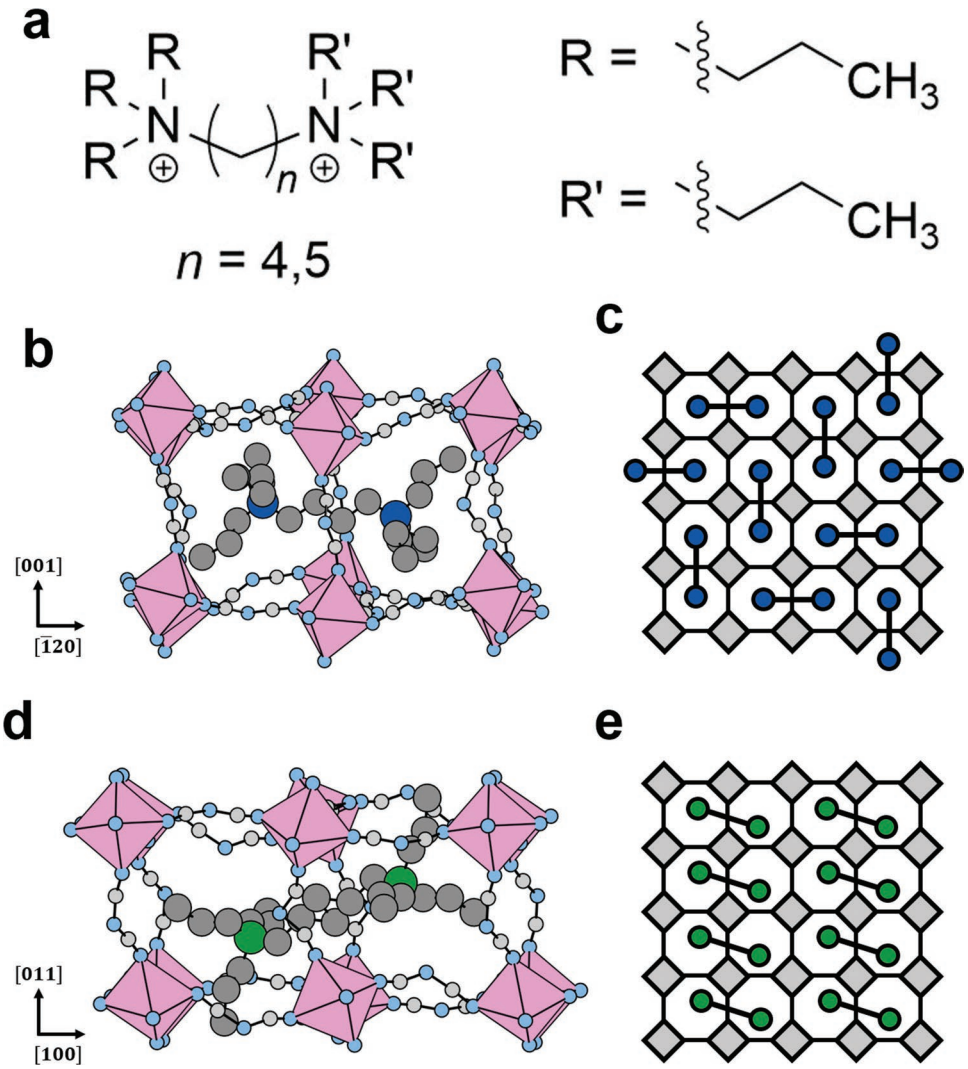

Figure 2. Crystal structures and A^{2+} cation order pattern in AB_2X_6 materials. Shown are a) a structural diagram of the molecules employed on the A-site and b) the crystal structures of $[TPC4TP]Mn_2(C_2N_3)_6$ and d) $[TPC5TP]Mn_2(C_2N_3)_6$ with emphasis on how the divalent A-site cations bridge two pseudocubic $Mn(C_2N_3)_3$ networks. c,e) For both materials a 2D order pattern of A^{2+} cations is observed. Depending on the separator length n of the $[R_3N(C_nH_{2n})NR_3]^{2+}$ cation, we observe a herringbone pattern ($n = 4$, c) or a head-to-tail pattern ($n = 5$, e). The hydrogen atoms are not shown for clarity. Color code for crystal structures: green/dark blue: A-cation nitrogen, gray: carbon, light-blue: X-anion nitrogen, pink: manganese. For visualization purposes, the size of the A-site atoms was increased.

the space diagonal and the AA stacking which both target to reduce steric interactions agree with this interpretation. This adaptive interplay between A^{2+} cations, their order pattern and the $[BX_3]^-$ network demonstrates the opportunities to synthetically engineer structural degrees of freedom in ReO_3-type coordination polymers to impart targeted responsive properties such as counterintuitive thermal and pressure responsive behavior and ferroelectricity.

2.3. Thermal Expansion Behavior and Compressibility

By drawing comparisons to materials with a herringbone motif and topologically related motifs such as $Ag_3[Co(CN)_6]$,[35] $KMn[Ag(CN)_2]_3$,[36] $[Zn_2(fu\text{-}bdc)_2dabco]$,[37] $[Fe(dpp)_2(NCS)_2]\cdot py$,[38] $InH(bdc)_2$,[39] and $MeOH\cdot H_2O$,[40] uniaxial negative thermal expansion (NTE) and negative linear compressibility (NLC) based on molecular hinging and rhombic network deformations can be anticipated. Variable temperature powder X-ray diffraction (T = 100–400 K) and high-pressure powder X-ray diffraction (p = ambient–0.4 GPa) were performed to obtain thermal expansion coefficients (α) and compressibilities (χ) for both materials, see Figure S20– S29, Supporting Information for details. For comparison reasons, lattice parameters were transformed into principal axes X_1, X_2, and X_3, see **Table 1** and Tables S7, S9, S11, and S13, Supporting Information. α and χ of both materials are in a similar magnitude with $[TPC4TP]Mn_2(C_2N_3)_6$ showing a slightly larger responsiveness toward temperature and pressure changes compared to $[TPC5TP]Mn_2(C_2N_3)_6$. This is ascribed to the lower packing density of $[TPC4TP]Mn_2(C_2N_3)_6$ which agrees with the trend in bulk moduli and shifts of characteristic IR bands of the $[C_2N_3]^-$

Table 1. Linear thermal expansion coefficients (MK^{-1}), compressibilities (TPa^{-1}) and calculated bulk moduli (GPa) of selected molecular framework materials in the ambient phase.

	α_{X1}	α_{X2}	α_{X3}	χ_{X1}	χ_{X2}	χ_{X3}	B_0	Ref.
$[TPC4TP]Mn_2(C_2N_3)_6$	−72(3)	113(7)	130(2)	−12(1)	58(2)	69(3)	6.3(4)	This work
$[TPC5TP]Mn_2(C_2N_3)_6$	−26(2)	69(2)	90(2)	6(1)	30(2)	53(1)	9.0(6)	This work
$Ag_3[Co(CN)_6]$	−126(1)[a]	138(1)[a]	138(1)[a]	−76(9)	115(8)	115(8)	6.5(3)	[35,41]
$KMn[Ag(CN)_2]_3$	61(2)	61(2)	−60(3)	−12(1)	33(1)	33(1)	12.7(11)	[36]
$[Zn_2(fu\text{-}L^1)_2dabco]$ (np)	−94	373	5					[37]
$[Fe(dpp)_2(NCS)_2]\cdot py$	−85(1)[a]	20(1)[a]	231(1)[a]	−10(2)	12(3)	53(4)	12.9(6)	[42,43]
$InH(bdc)_2$	64(3)	64(3)	−35(2)	102	102	−62	6.8	[39,44]
$MeOH{\cdot}H_2O$	−19(1)	85(5)	230(19)	−3(2)	32(1)	108(1)	3.8(1)	[40]
$[(C_3H_7)_4N]Mn(C_2N_3)_3$				54(2)	54(2)	8(1)	8.1(11)	[45]
$[C(NH_2)_3]Cd(HCOO)_3$	−17(1)	−17(1)	106(3)	3(1)	3(1)	21(1)	25.7(17)	[46,47]

Abbrv. fu = functionalized, L^1 = 2,5-bis(2-methoxyethoxy)benzene-1,4-dicarboxylate, np = narrow pore, dpp = dipyrido[3,2-*a*:2′3′-*c*]phenazine, py = pyridine, bdc = benzene-1,4-dicarboxylate; [a]recalculated from reported heating/compression lattice parameters using the software PASCal.[48]

linker, see Table 1 and Figure S10 and Table S14, Supporting Information for details.

Looking at $[TPC4TP]Mn_2(C_2N_3)_6$, large uniaxial NTE and NLC behavior is observed along X_1 with $\alpha_{X1} = -71.63 \pm 2.65\ MK^{-1}$ and $\chi_{X1} = -11.73 \pm 1.13\ TPa^{-1}$. X_1 points along [304] in the unit cell which is the space diagonal of a $2 \times 2 \times 2$ $[M(C_2N_3)]^-$ unit and the direction in which counter-intuitive material response based on a 3D hinging of A-site cations is expected, see **Figure 3**e and Figure S14, Supporting Information for a mechanistic illustration. For X_2 and X_3 uniaxial expansion and linear compressibility is observed, overall compensating for total framework deformation. This observation suggests that A-site hinging combined with a rhombic network distortion is suitable to rationalize uniaxial NTE and NLC behavior of $[TPC4TP]Mn_2(C_2N_3)_6$. To further support this interpretation, temperature-dependent single crystal X-ray diffraction for $[TPC4TP]Mn_2(C_2N_3)_6$ at 100, 205, and 310 K was performed, see Table S3, Supporting Information. An increasing dihedral angle for two A-site cations ($\measuredangle_{100\,K} = 81.71(7)°$ to $\measuredangle_{310\,K} = 83.8(3)°$) and decreasing Mn-Mn distance along [304] are observed which corroborates the interpretation of thermal and pressure responsiveness of $[TPC4TP]Mn_2(C_2N_3)_6$ based on a hinging mechanism. Importantly, it is the synergistic interplay of the A^{2+} cations' herringbone order pattern and the constraining $[BX_3]^-$ network that causes NTE and NLC based on a herringbone-based hinging mechanism in these framework materials. A herringbone motif alone is only an insufficient criteria as it was recently shown for the molecular crystals $Cu(acac)_2$ ($acac^{2-}$ = acetylacetonato)[49] and the series of linear acenes.[50] Comparing the sizes of α_{X1} and χ_{X1} of $[TPC4TP]Mn_2(C_2N_3)_6$ with other molecular perovskites and coordination polymers (Table 1), the observed NLC coefficients and uniaxial NTE coefficents are large and to our knowledge $[TPC4TP]Mn_2(C_2N_3)_6$ is the first ReO_3-type coordination polymer with a large NLC coefficient of the ambient phase.

In contrast, for $[TPC5TP]Mn_2(C_2N_3)_6$ we only find moderate uniaxial NTE along X_1 with $\alpha_{X1} = -26.01 \pm 1.81\ MK^{-1}$ and close to zero linear compressibility along X_1 which is approximately along the space-diagonal of a $1 \times 2 \times 2$ pseudocubic $[Mn(C_2N_3)_3]^-$ network. Therefore, uniaxial NTE propagates perpendicular to the skewed head-to-tail arranged A-cations in [401] direction and is presumably based on a lamellar-type movement of the A-site molecules and a related rhombic distortion of the network. The absence of NLC behavior as a formally reversed structural distortion of uniaxial NTE is less clear; however, the different responses toward temperature and pressure changes illustrate that a clear mechanism that provides a well-defined minimum energy structural distortion is not provided by a head-to-tail arrangement of A-site cations when compared with a herringbone arrangement.

3. Conclusion

In conclusion, we introduce a new family of AB_2X_6 coordination polymers based on a ReO_3-type network. The synthesis of two representatives is reported in which the divalent A-site cation bridges two pseudocubic $[BX_3]^-$ cages. This introduces the spatial orientation of divalent A^{2+} cations as a geometric degree of freedom, while maintaining all structural degrees of freedom as known from molecular perovskites such as (unconventional) octahedral tilts and shifts, and a variable A-site cation chemistry. The type of A^{2+} cation order pattern and its interplay with distortion modes of the 3D network are suitable to rationalize the mechanical properties of the materials. For $[TPC4TP]Mn_2(C_2N_3)_6$, the herringbone motif couples with structural distortions of the 3D network, providing a clear low-energy pathway for structural distortions as a function of temperature and pressure variation. In going forward, the chemical variability of divalent $[R'_3N(CH_2)_nNR_3]^{2+}$ cations is promising to impart new, yet unknown A^{2+} order pattern and therewith coupling schemes that determine the stimuli-responsive material properties. In particular, the use of nonsymmetric cations based on different R' and R functionalities is intriguing, where the use of R = –H and R' = $-(C_3H_7)$ seems promising. Such an A-site cation incorporates one A-site end that is formally too small for forming a perovskite motif, which might introduce packing frustration coupled to extreme or counter-intuitive stimuli-responsive properties.

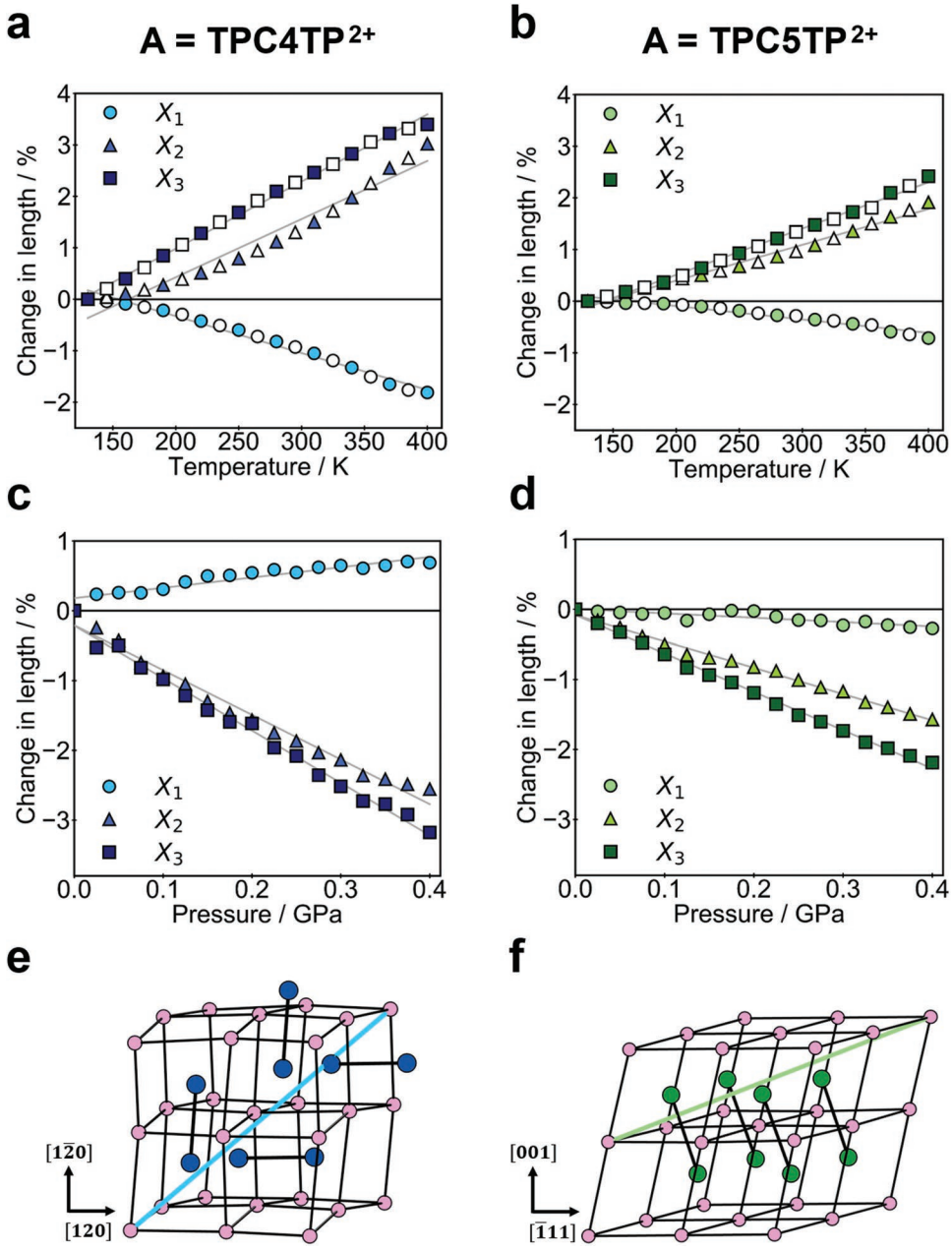

Figure 3. Temperature and pressure dependent structural behavior of AB_2X_6 coordination polymers. Shown are the evolution of principal axes as a function of temperature and pressure. For A = TPC4TP^{2+}, uniaxial NTE and NLC along X_1 is observed, whilst for A = TPC5TP^{2+} uniaxial NTE and positive compressibilities are found. For temperature-dependent data, filled and open symbols represent heating and cooling, respectively. e,f) show a $2 \times 2 \times 2$ perovskite-type unit with the particular direction of propagation for the principal axis X_1 illustrated, respectively. Color code: green/dark blue: A-cation N, pink: Mn. Note that the black lines are only a guide to the eye to indicate the perovskite-type connectivity and do not represent real chemical bonds.

The herein presented materials are conceptually related to the work by Telfer,[51] where geometric degrees of freedom were introduced by controlled interpenetration of MUF-9. This and many other examples highlight that decomposing a coordination networks' structure into (structural) degrees of freedom is a material class overarching conceptualization to rationalize stimuli-responsive material behavior, and in the future, may serve as a powerful design principle. As a concept, it represents a natural development of rigid-body guidelines such as the reticular chemistry approach[52] and the Goldschmidt tolerance factor approach for (molecular) perovskites[53] to control responsive properties through crystal structure engineering. Importantly, when considering photoactive linker molecules or catalytically active structural entities in coordination polymers such as MOFs as chemical degrees of freedom, the combination of structural with chemical degrees of freedom seems intriguing to rationally synthesize multifunctional materials with potentially new properties. Research examples exist that can be understood within this framework such as switchable catalysts based on flexible MOFs,[54] energy transfer processes

in photoactive MOFs,[55] and the geometric arrangement of redox-active linker molecules in electrically conductive MOFs[56] amongst other examples. To advance this concept to a practically useful guideline, the identification of new structural degrees of freedom, learning about the design of their interplay, and impact on stimuli-responsive properties is key, to which this work provides an important step.

4. Experimental Section

All experimental and analytical data including a detailed description of synthesis procedures for the precursor compounds as well as details on structure determination can be found in Supporting Information. This also includes experimental details for data collection at the synchrotron facilities Diamond Light Source Ltd., UK and DESY, Germany. The reported crystal structures are available through the Cambridge Crystallographic Database listed with the respective entry numbers as can be found in Supporting Information.

Statistical Analysis: All experimental data were evaluated with respect to relevant error calculations and measurement uncertainties and when appropriate, the results of error analysis are discussed in Supporting Information.

Supporting Information

Supporting Information is available from the Wiley Online Library or from the author.

Acknowledgements

S.B. would like to thank the Hanns–Seidel-Foundation for financial support through a Ph.D. fellowship. G.K. would like to thank the "Fonds der Chemischen Industrie" for support through the Liebig Fellowship scheme. K.H. thanks the "Fonds der Chemischen Industrie" for a Ph.D. fellowship. J.K.Z. acknowledges support from Academia Iuvenum, Wroclaw University of Science and Technology. The authors would like to acknowledge beamtime at the Diamond Light Source Ltd., UK (experiment CY22477-2, beamline I15). The authors acknowledge DESY (Hamburg, Germany), a member of the Helmholtz Association HGF, for the provision of experimental facilities. Parts of this research were carried out at PETRA III (experiment I-20191507) and the authors would like to thank Martin Etter and Alexander Schökel for assistance in using beamline P02.1 for data collection. Additionally, the measurements at DESY leading to this results has been supported with travel reimbursement from DESY, for which the authors are grateful.

Open access funding enabled and organized by Projekt DEAL.

Conflict of Interest

The authors declare no conflict of interest.

Author Contributions Statement

S.B. and G.K. designed the study, analyzed experimental outcomes, and wrote the manuscript. K.H., P.V., and D.D. assisted in synchrotron data collection and interpretation of results. J.K.Z conducted the SHG measurements and D.M. assisted with single crystal diffraction. In addition to continuous scientific exchange, all authors contributed to proof-reading and revisions of the manuscript.

Data Availability Statement

The data that support the findings of this study are available in the supplementary material of this article

Keywords

coordination polymers, materials chemistry, negative linear compressibility, structural degrees of freedom, uniaxial negative thermal expansion

Received: May 10, 2022
Revised: June 27, 2022
Published online: August 8, 2022

[1] N. Hanikel, M. S. Prévot, O. M. Yaghi, *Nat. Nanotechnol.* **2020**, *15*, 348.
[2] J. M. Bermúdez-García, M. Sánchez-Andújar, S. Castro-García, J. López-Beceiro, R. Artiaga, M. A. Señarís-Rodríguez, *Nat. Commun.* **2017**, *8*, 15715.
[3] S. Krause, V. Bon, I. Senkovska, U. Stoeck, D. Wallacher, D. M. Többens, S. Zander, R. S. Pillai, G. Maurin, F.-X. Coudert, S. Kaskel, *Nature* **2016**, *532*, 348.
[4] A. B. Cairns, J. Catafesta, C. Levelut, J. Rouquette, A. van der Lee, L. Peters, A. L. Thompson, V. Dmitriev, J. Haines, A. L. Goodwin, *Nat. Mater.* **2013**, *12*, 212.
[5] N. C. Burtch, S. J. Baxter, J. Heinen, A. Bird, A. Schneemann, D. Dubbeldam, A. P. Wilkinson, *Adv. Funct. Mater.* **2019**, *29*, 1904669.
[6] A. P. Katsoulidis, D. Antypov, G. F. S. Whitehead, E. J. Carrington, D. J. Adams, N. G. Berry, G. R. Darling, M. S. Dyer, M. J. Rosseinsky, *Nature* **2019**, *565*, 213.
[7] S. Horike, S. S. Nagarkar, T. Ogawa, S. Kitagawa, *Angew. Chem., Int. Ed.* **2020**, *59*, 6652.
[8] C. L. Hobday, G. Kieslich, *Dalton Trans.* **2021**, *50*, 3759.
[9] S. Krause, N. Hosono, S. Kitagawa, *Angew. Chem., Int. Ed.* **2020**, *59*, 15325.
[10] H. L. B. Boström, A. L. Goodwin, *Acc. Chem. Res.* **2021**, *54*, 1288.
[11] M. J. Pitcher, P. Mandal, M. S. Dyer, J. Alaria, P. Borisov, H. Niu, J. B. Claridge, M. J. Rosseinsky, *Science* **2015**, *347*, 420.
[12] J. H. Jung, Z. Fang, J. P. He, Y. Kaneko, Y. Okimoto, Y. Tokura, *Phys. Rev. Lett.* **2003**, *91*, 056403.
[13] H. L. B. Boström, M. S. Senn, A. L. Goodwin, *Nat. Commun.* **2018**, *9*, 2380.
[14] Q. Chen, H. Zhou, Z. Hong, S. Luo, H.-S. Duan, H.-H. Wang, Y. Liu, G. Li, Y. Yang, *J. Am. Chem. Soc.* **2014**, *136*, 622.
[15] P. Iacomi, J. S. Lee, L. Vanduyfhuys, K. H. Cho, P. Fertey, J. Wieme, D. Granier, G. Maurin, V. van Speybroeck, J.-S. Chang, P. G. Yot, *Chem. Sci.* **2021**, *12*, 5682.
[16] P. Vervoorts, J. Keupp, A. Schneemann, C. L. Hobday, D. Daisenberger, R. A. Fischer, R. Schmid, G. Kieslich, *Angew. Chem., Int. Ed.* **2021**, *60*, 787.
[17] Y.-S. Su, E. S. Lamb, I. Liepuoniute, A. Chronister, A. L. Stanton, P. Guzman, S. Pérez-Estrada, T. Y. Chang, K. N. Houk, M. A. Garcia-Garibay, S. E. Brown, *Nat. Chem.* **2021**, *13*, 278.
[18] A. Simonov, T. de Baerdemaeker, H. L. B. Boström, M. L. Ríos Gómez, H. J. Gray, D. Chernyshov, A. Bosak, H.-B. Bürgi, A. L. Goodwin, *Nature* **2020**, *578*, 256.
[19] F. M. Amombo Noa, E. Svensson Grape, S. M. Brülls, O. Cheung, P. Malmberg, A. K. Inge, C. J. McKenzie, J. Mårtensson, L. Öhrström, *J. Am. Chem. Soc.* **2020**, *142*, 9471.
[20] V. Guillerm, D. Maspoch, *J. Am. Chem. Soc.* **2019**, *141*, 16517.

[21] F. Haase, G. A. Craig, M. Bonneau, K. Sugimoto, S. Furukawa, *J. Am. Chem. Soc.* **2020**, *142*, 13839.
[22] J. J. Oppenheim, G. Skorupskii, M. Dincă, *Chem. Sci.* **2020**, *11*, 11094.
[23] W. Li, Z. Wang, F. Deschler, S. Gao, R. H. Friend, A. K. Cheetham, *Nat. Rev. Mater.* **2017**, *2*, 3.
[24] Y. Wu, S. Shaker, F. Brivio, R. Murugavel, P. D. Bristowe, A. K. Cheetham, *J. Am. Chem. Soc.* **2017**, *139*, 16999.
[25] J. A. Schlueter, J. L. Manson, U. Geiser, *Inorg. Chem.* **2005**, *44*, 3194.
[26] P. Jain, N. S. Dalal, B. H. Toby, H. W. Kroto, A. K. Cheetham, *J. Am. Chem. Soc.* **2008**, *130*, 10450.
[27] H. L. B. Boström, *CrystEngComm* **2020**, *22*, 961.
[28] W.-J. Xu, S.-L. Chen, Z.-T. Hu, R.-B. Lin, Y.-J. Su, W.-X. Zhang, X.-M. Chen, *Dalton Trans.* **2016**, *45*, 4224.
[29] I. E. Collings, M. Bykov, E. Bykova, M. Hanfland, S. van Smaalen, L. Dubrovinsky, N. Dubrovinskaia, *CrystEngComm* **2018**, *20*, 3512.
[30] W. Wei, W. Li, K. T. Butler, G. Feng, C. J. Howard, M. A. Carpenter, P. Lu, A. Walsh, A. K. Cheetham, *Angew. Chem., Int. Ed.* **2018**, *57*, 8932.
[31] S. Burger, S. Grover, K. T. Butler, H. L. B. Boström, R. Grau-Crespo, G. Kieslich, *Mater. Horiz.* **2021**, *8*, 2444.
[32] J. M. Bermúdez-García, M. Sánchez-Andújar, M. A. Señarís-Rodríguez, *J. Phys. Chem. Lett.* **2017**, *8*, 4419.
[33] L. Xin, Z. Zhang, M. A. Carpenter, M. Zhang, F. Jin, Q. Zhang, X. Wang, W. Tang, X. Lou, *Adv. Funct. Mater.* **2018**, *28*, 1806013.
[34] M.-L. Tong, J. Ru, Y.-M. Wu, X.-M. Chen, H.-C. Chang, K. Mochizuki, S. Kitagawa, *New J. Chem.* **2003**, *27*, 779.
[35] A. L. Goodwin, M. Calleja, M. J. Conterio, M. T. Dove, J. S. O. Evans, D. A. Keen, L. Peters, M. G. Tucker, *Science* **2008**, *319*, 794.
[36] A. B. Cairns, A. L. Thompson, M. G. Tucker, J. Haines, A. L. Goodwin, *J. Am. Chem. Soc.* **2012**, *134*, 4454.
[37] S. Henke, A. Schneemann, R. A. Fischer, *Adv. Funct. Mater.* **2013**, *23*, 5990.
[38] H. J. Shepherd, T. Palamarciuc, P. Rosa, P. Guionneau, G. Molnár, J.-F. Létard, A. Bousseksou, *Angew. Chem., Int. Ed.* **2012**, *51*, 3910.
[39] Q. Zeng, K. Wang, B. Zou, *J. Am. Chem. Soc.* **2017**, *139*, 15648.
[40] A. D. Fortes, E. Suard, K. S. Knight, *Science* **2011**, *331*, 742.
[41] A. L. Goodwin, D. A. Keen, M. G. Tucker, *Proc. Natl. Acad. Sci. USA* **2008**, *105*, 18708.
[42] J. Kusz, M. Zubko, A. Fitch, P. Gütlich, *Z. Kristallogr.* **2011**, *226*, 576.
[43] J. N. Grima, R. Caruana-Gauci, D. Attard, R. Gatt, *Proc. R. Soc. A* **2012**, *468*, 3121.
[44] I. E. Collings, M. G. Tucker, D. A. Keen, A. L. Goodwin, *CrystEngComm* **2014**, *16*, 3498.
[45] M. Mączka, I. E. Collings, F. F. Leite, W. Paraguassu, *Dalton Trans.* **2019**, *48*, 9072.
[46] I. E. Collings, J. A. Hill, A. B. Cairns, R. I. Cooper, A. L. Thompson, J. E. Parker, C. C. Tang, A. L. Goodwin, *Dalton Trans.* **2016**, *45*, 4169.
[47] H. Gao, C. Li, L. Li, W. Wei, Y. Tan, Y. Tang, *Dalton Trans.* **2020**, *49*, 7228.
[48] M. J. Cliffe, A. L. Goodwin, *J. Appl. Cryst.* **2012**, *45*, 1321.
[49] A. J. Brock, J. J. Whittaker, J. A. Powell, M. C. Pfrunder, A. Grosjean, S. Parsons, J. C. McMurtrie, J. K. Clegg, *Angew. Chem., Int. Ed.* **2018**, *57*, 11325.
[50] S. Haas, B. Batlogg, C. Besnard, M. Schiltz, C. Kloc, T. Siegrist, *Phys. Rev. B* **2007**, *76*, 843.
[51] A. Ferguson, L. Liu, S. J. Tapperwijn, D. Perl, F.-X. Coudert, S. van Cleuvenbergen, T. Verbiest, M. A. van der Veen, S. G. Telfer, *Nat. Chem.* **2016**, *8*, 250.
[52] R. Freund, S. Canossa, S. M. Cohen, W. Yan, H. Deng, V. Guillerm, M. Eddaoudi, D. G. Madden, D. Fairen-Jimenez, H. Lyu, L. K. Macreadie, Z. Ji, Y. Zhang, B. Wang, F. Haase, C. Wöll, O. Zaremba, J. Andreo, S. Wuttke, C. S. Diercks, *Angew. Chem., Int. Ed.* **2021**, *60*, 23946.
[53] G. Kieslich, S. Sun, A. K. Cheetham, *Chem. Sci.* **2014**, *5*, 4712.
[54] S. Yuan, L. Zou, H. Li, Y.-P. Chen, J. Qin, Q. Zhang, W. Lu, M. B. Hall, H.-C. Zhou, *Angew. Chem., Int. Ed.* **2016**, *55*, 10776.
[55] D. E. Williams, J. A. Rietman, J. M. Maier, R. Tan, A. B. Greytak, M. D. Smith, J. A. Krause, N. B. Shustova, *J. Am. Chem. Soc.* **2014**, *136*, 11886.
[56] T. C. Narayan, T. Miyakai, S. Seki, M. Dincă, *J. Am. Chem. Soc.* **2012**, *134*, 12932.